ce/papers Proceedings in civil engineering

Ernst & Sohn A Wiley Brand

ORIGINAL ARTICLE

eurosteel AMSTERDAM 2023

Ernst & Sohn A Wiley Brand

Load-carrying capacity of MAG butt and fillet welded joints on high-strength structural steels of grade S960QL and S960MC

Oliver Brätz[1] | Mareike von Arnim[2] | Stefan Eichler[3] | Andreas Gericke[1] | Knuth-Michael Henkel[1] | Jörg Hildebrand[3] | Jean Pierre Bergmann[3] | Ulrike Kuhlmann[2]

Correspondence

Dr. Oliver Brätz
Fraunhofer Institute for Large Structures in Production Engineering IGP
Albert-Einstein-Straße 30
18059 Rostock, Germany
Email: oliver.braetz@igp.fraunhofer.de

[1] Fraunhofer IGP, Rostock, Germany
[2] University of Stuttgart, Institute of Structural Design, Stuttgart, Germany
[3] Technische Universität Ilmenau, Department of Mechanical Engineering, Production Technology Group, Ilmenau, Ilmenau, Germany

Abstract

The use of high-strength structural steels brings great advantages in constructions regarding material requirements, weight reduction and productivity. Different steel grades within the S960 range are commercially available but not yet represented in Eurocode 3. The weldability of these steels is limited to smaller process windows to ensure the high material properties. In contrast to steels with moderate strength, there is a considerable risk of softening in the heat-affected zone causing a strength reduction of the connection. By now, the current EN 1993-1-12 only extends the design rules to cover steel grades up to S700. Therefore, the potential of these high-strength steels cannot be used to its full extent in structural engineering. This study, made within a steel application research project (FOSTA P 1507), deals with the weldability and load-carrying capacity of butt and fillet welded joints of S960QL and S960MC produced by gas-shielded metal arc welding. The influence of different bevel geometry, filler metal, and plate thicknesses was investigated. To extend the design rules up to S960, a need of an amendment was found for some combinations.

Keywords

ultra-high strength steel UHSS, Eurocode 3, weldability, tensile test, HAZ softening

1 Introduction

The material properties of weldable structural steels have been developed considerably over the past decades. Steels of grade S960 showing nominal yield strengths of $R_{eH} \geq 960$ MPa depending on the thickness, also termed as ultra-high strength steel (UHSS), are available. Due to significant strength-to-weight advantages the use of UHSS offers an enormous potential for material and cost saving in structural application. Nonetheless, it is known that they show a limited weldabilty, and due to the typical thermal influence of arc welding a local strength reduction can occur in the heat-affected zone (HAZ). This softened zone can reduce the load-carrying capacity of the welded connection and may lead to a premature failure in the HAZ [1]-[5]. The achieved load-carrying capacities are found to be sometimes more than 15 % lower than the tensile strength of the high-strength parent metal [6]. However it is known that the weldability and softening characteristics can significantly differ based on the alloy design and manufacturing method [4][7][8]. At present, for full penetration butt welds there is usually no necessity of separately verifying its design resistance, provided that the weld is made with a suitable consumable ensuring a minium yield and tensile strength not less than those specified for the parent metal; i.e., the verification of the design resistance based on the nominal material properties acc. to EN 1993-1-1 [9] is sufficient. The current codes EN 1993-1-8 [10] and EN 1993-1-12 [11] are inadequate for high-strength butt welds, and in some cases the design is on the unsafe side. The standards do not take into account the special behaviour of UHSS, i.e. formation of a soft zone.

A new design approach has been developed in [6] that allows economical and safe design of high-strength butt welds, see Eq. (1).

$$\sigma_{w,Rd} = \frac{0.85 \cdot (0.9\, f_u) + 0.15\, f_{u,FM}}{\gamma_{M2}} \quad (1)$$

with the following factors:

f_u nominal ultimate tensile strength, parent material
$f_{u,FM}$ nominal ultimate tensile strength of the filler metal
γ_{M2} partial factor (1.25 for welds)

The welding-related softening is considered by a factor of 0.9. The equation applies to full penetration butt welds with steels grades higher than S460 and up to S700. It is possible to use filler metals with lower (undermatching), equal (matching) and higher (overmatching) strength compared to the base metal. For steel grade S460 Eq. (1)

https://doi.org/10.1002/cepa.2478 wileyonlinelibrary.com/journal/cepa

is valid for undermatching or overmatching. This design concept was accepted by the responsible working group CEN TC250/SC 3/WG 8 for FprEN 1993-1-8:2023 [12]. Since the new edition of prEN 1993-1-12 [13] will also be extended up to S960 steel grades, tests on butt welds of these steel grades are conducted in a study as part of a joint research project, see acknowledgement. With the results obtained, the design concept will be extended.

The design resistance of fillet welds determined by using the directional method is based on the equivalent engineering stress derived by Eq. (2).

$$\sigma_{v,Ed} = \sqrt{\sigma_{\perp}^2 + 3 \cdot (\tau_{\perp}^2 + \tau_{\parallel}^2)} \qquad (2)$$

where

$\sigma_{\perp}$ is the normal stress perpendicular to the throat

$\tau_{\perp}$ is the shear stress in the plane of the throat perpendicular to the axis of the weld

$\tau_{\parallel}$ is the shear stress in the plane of the throat parallel to the axis of the weld

The normal stress along the axis of the weld $\sigma_{\parallel}$ can be ignored when verifying the design resistance of fillet welds. The design resistance of the fillet weld is sufficient if the following Eq. (3) are both satisfied:

$$\sigma_{v,Ed} \leq \frac{f_u}{\beta_w \cdot \gamma_{M2}} \quad \text{and} \quad \sigma_{\perp} \leq \frac{0.9\, f_u}{\gamma_{M2}} \qquad (3)$$

where

β_w is the appropriate correlation factor for fillet welds acc. to Table 6.1 in [12]

Alternatively, the design resistance of a fillet weld in connections of steel grades from S460 up to S700, and with different parent and filler metal strength, should be taken as sufficient if the following Eq. (4) are satisfied. In this case f_u is the nominal ultimate tensile strength of the parent metal, which is of lower strength grade.

$$\sigma_{v,Ed} \leq \frac{0.25\, f_u + 0.75\, f_{u,FM}}{\beta_{w,mod} \cdot \gamma_{M2}} \quad \text{and} \quad \sigma_{\perp} \leq \frac{0.9\, f_u}{\gamma_{M2}} \qquad (4)$$

where

$\beta_{w,mod}$ is a modified correlation factor that depends on the filler metal strength acc. to Table 6.2 in [12] (e.g. 0.85 for "G46", 1.09 for "G69", 1.19 for "G89" or "T89")

2 Experimental methods

2.1 Materials and welding of samples

As base materials two different structural steels with the same high nominal yield strengths of $R_{eH} \geq 960$ MPa were used. One the one hand a structural steel in quenched and tempered condition acc. to EN 10025-6-S960QL (1.8933) and a thermomechanical rolled steel for cold forming acc. to EN 10149-2-S960MC (1.8799) on the other. As welding consumables wire electrodes of different strength class G46, G69 and G89 as well as a tubular cored electrode T89 were used. The standardized specifications and actual mechanical properties of the used materials are listed in Table 1. The chemical composition of the used materials and the metallurgical weldability expressed by their carbon equivalents are given in Table 2. Since the used G89 is marked as filler material for fine grain structural steels above S890 and it shows mechanical properties in the range of S960 grades, it is considered as a quasi-matching consumable even though its symbol for tensile properties formally indicates only $f_{u,FM}$ = 940 N/mm² acc. to [12]. This is attributed to the fact that 89 is the maximum strength class for standardized wire electrodes for GMAW of high strength steels in ISO 16834.

Table 1 Mechanical properties of used materials and filler metals, for steel plates transversal to rolling direction

Material	Specification	$R_{p0,2}$ in MPa	R_m in MPa	A in %	KV_2 in J (at °C)
S960QL, t10	EN 10025-6-S960QL	1036	1077	11	27 (-40)
S960QL, t20	EN 10025-6-S960QL	1045	1074	14	138 (-40)
S960MC, t10	EN 10149-2-S960MC	965	1022	13	n.a.
G46	ISO 14341-A G 46 5 M21 4Si1	525	598	22	83 (-50)
G69	ISO 16834-A G 69 6 M21 Mn4Ni1.5CrMo	761	806	18	81 (-60)
G89	ISO 16834-A G 89 6 M21 Mn4Ni2CrMo	1040	1108	15	62 (-60)
T89	ISO 18276-A T 89 4 Z M M21 3 H5	931	993	19	82 (-40)

In this study, butt welded joints and longitudinal fillet welded joints were investigated. The weld samples were produced by metal active gas (MAG) / gas metal arc welding (GMAW) using active gas with solid wire electrode (135) or metal cored electrode (138). A mixed gas in accordance with ISO 14175 – M21 – ArC – 82/18 was used as shielding gas. The processes were all carried out with standard arc control and direct current electrode positive polarity. The transfer mode was short circuiting or spray. A collaborative robot (Universal Robots, UR10) equipped with MAG-welding machine (Lorch, S5 SpeedPulse) was used to perform automatic welding with manual teaching of every run, see Figure 1.

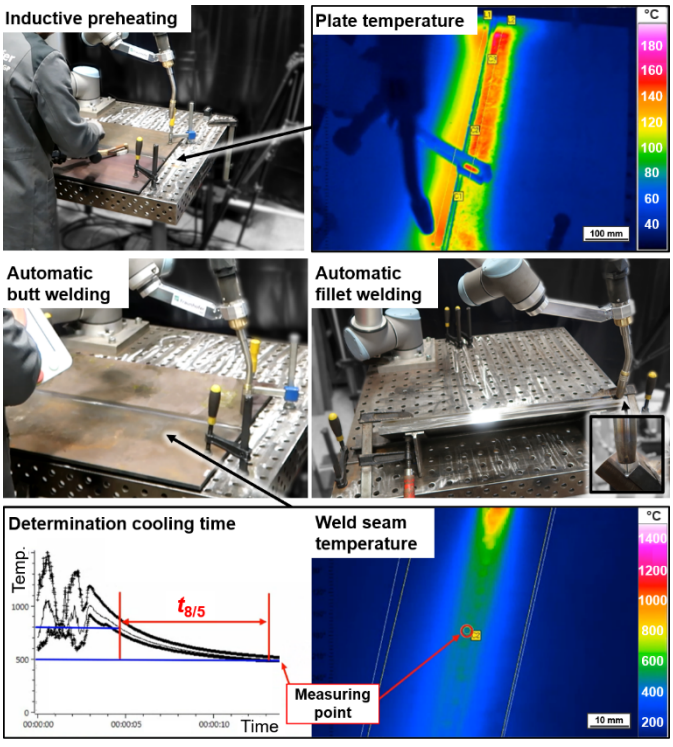

Figure 1 Welding of samples with preheating and measurement of cooling time

The butt welded joints were carried out by multi-pass welding, whereas the fillet welds were realized by single-

Table 2 Chemical composition of used materials and filler metals

Material	C in wt%	Si in wt%	Mn in wt%	P in wt%	S in wt%	Cr in wt%	Ni in wt%	Mo in wt%	Cu in wt%	Al in ppm	Ti in ppm	B in ppm	Nb in ppm	V in ppm	Zr in ppm	N in ppm	*CEV* [1] in %	*CET* [2] in %
S960QL, t10	0.167	0.29	1.39	0.009	0.001	0.28	0.123	0.52	0.103	270	20	28	260	20	10	50	0.57	0.38
S960QL, t20	0.165	0.28	1.08	0.011	0.001	0.19	0.035	0.52	0.022	n.a.	180	14	10	10	2	n.a.	0.49	0.34
S960MC, t10	0.079	0.33	1.64	0.007	0.001	0.65	0.032	0.31	0.014	430	120	14	330	750	n.a.	56	0.56	0.31
G46	0.080	0.96	1.67	0.009	0.009	0.03	0.010	0.01	0.006	20	110	4	10	20	n.a.	n.a.	0.37	0.25
G69	0.080	0.56	1.65	0.006	0.011	0.24	1.580	0.47	0.028	30	640	10	40	30	n.a.	n.a.	0.60	0.34
G89	0.110	0.83	1.78	0.006	0.011	0.37	2.240	0.57	0.013	30	750	1	30	30	n.a.	n.a.	0.75	0.42
T89	0.090	0.51	1.29	0.008	0.014	0.55	2.800	0.82	n.a.	n.a.	n.a.	n.a.	n.a.	n.a.	n.a.	n.a.	0.77	0.40

[1] Carbon equivalent acc. to IIW / EN 1011-2 – Method A: *CE* = *CEV* = C + Mn/6 + (Cr + Mo + V)/5+ (Ni + Cu)/15 in %

[2] Carbon equivalent acc. to EN 1011-2 – Method B: *CET* = C + (Mn + Mo)/10 + (Cr + Cu)/20+ Ni/40 in %

layer welding. For the butt welded joints a single-V or double-V grooves with an included angle of 60° and 2 mm root face were prepared. An appropriate preheating was determined in accordance with EN 1011-2 [14] and supplementary technical rules [16] based on the actual base metal and filler metal composition, the welding heat input, and the joint geometry. This common practice is applied to avoid hydrogen-assisted cold cracking. To achieve equal cooling conditions upon welding, the highest determined preheating temperature was set for all weld samples with same geometry. For butt weld samples with a thickness of t = 10 mm a preheating of T_P = 120 °C was defined. For the butt weld and fillet weld samples with larger thickness of t = 20 mm T_P = 150 °C was defined.
To ensure a sufficient heat input that causes high cooling times and a relatively strong thermal impact on the parent material appropriate welding parameters were chosen, cf. [15]. The aim was to achieve a nominal weld metal cooling time interval from 800 to 500 °C of $t_{8/5}$ = 8 s for the butt welds. Whereas, for the fillet welds an equal throat thickness of a = 4 mm was aimed. During welding, the cooling times $t_{8/5}$ were determined by using an infrared thermographic camera (InfraTec, VarioCAM hr 675S) and temperature measurements on the weld seam surface, see Figure 1. The used welding parameters and the measured cooling times are listed in Table 3.

Table 3 Welding parameters, measured mean values

Joint / Sample	Base material	Weld. cons.	Current *I* in A	Voltage *U* in V	W. speed *v* in m/min	Arc energy [1] *E* in kJ/mm	Cool. T. $t_{8/5}$ in s
lap joint long. fillet weld	S960QL, t20	G46	320	28.6	0.40	1.4	6.2
		G69	327	28.5	0.40	1.4	5.8
		G89	305	28.8	0.40	1.3	5.4
		T89	342	28.0	0.40	1.4	7.2
V groove trans. butt weld	S960MC, t10	G46	259	24.3	0.50	0.8	7.1
		G89	243	24.8	0.46	0.8	7.4
	S960QL, t10	G46	255	24.5	0.46	0.8	7.9
		G89	248	24.6	0.46	0.8	7.5
	S960QL, t20	G46	312	28.0	0.45	1.2	7.1
		G89	300	28.3	0.45	1.1	6.8
DV groove trans. butt weld	S960MC, t10	G46	273	24.5	0.45	0.9	9.3
		G89	296	24.0	0.45	1.0	10.5
	S960QL, t10	G46	286	23.5	0.45	0.9	9.4
		G89	276	23.7	0.45	0.9	8.9
	S960QL, t20	G46	318	27.8	0.45	1.2	7.2
		G89	313	27.8	0.45	1.2	7.1

[1] Arc energy as heat input acc. to ISO/TR 17671-1 neglecting the thermal efficiency factor

2.2 Testing of joints

Since the weldability and the characteristic of the formed soft zone in the HAZ are of essential interest to discuss the entire joint performance and for the design concept, the hardness distribution in section was closely analysed by high-resolution hardness mapping over the entire joint area. A hardness testing scanner (BAQ, UT 200) based on the ultrasonic contact impedance (UCI) measuring method allowing the value output in the scale of Vickers was used. The distance between individual impressions was set to 100 µm in a square-shaped grit. The applied test method was firstly validated by comparative measurements using a standard Vickers indenter instrument in the micro test range HV0.1, cf. [17].
To determine the maximum load capacity of the welds two different geometries of the test specimens were chosen, see Figure 2.

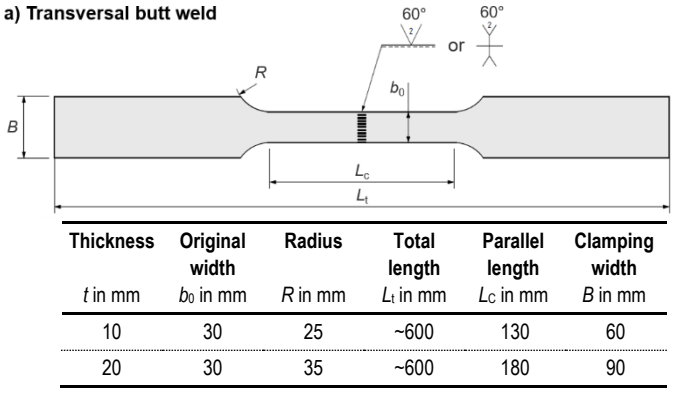

Thickness *t* in mm	Original width b_0 in mm	Radius *R* in mm	Total length L_t in mm	Parallel length L_C in mm	Clamping width *B* in mm
10	30	25	~600	130	60
20	30	35	~600	180	90

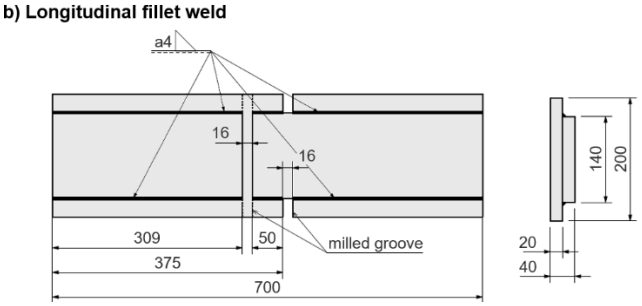

Figure 2 Test specimens for tensile tests of a) transversal butt welded joint and b) longitudinal fillet welds

Waisted transverse tensile test specimens with welds being ground flush were used for butt weld testing. To investigate the load-carrying capacity of longitudinal fillet welds a special geometry of the specimens with high stiffness and exclusive weld seam loading was defined.

The tensile tests were conducted as open loop method with a constant crosshead separation rate of v_c = 2 mm/min for t = 10 mm and v_c = 3 mm/min for t = 20 mm at room temperature. The local deformation was measured optically with a stereo camera system (GOM, ARAMIS) based on grayscale analysis. The surfaces of the samples were painted with a random speckle pattern before, see Figure 3.

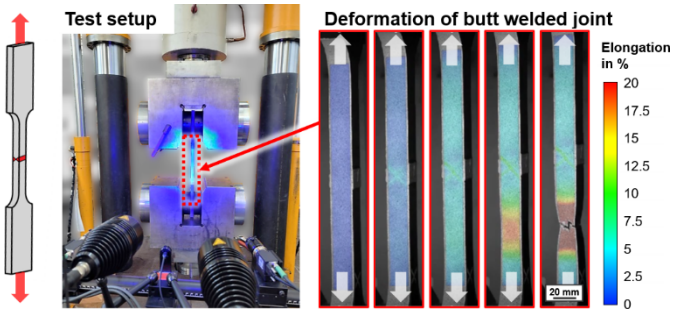

Figure 3 Experimental setup for tensile tests of butt welded joints with optical local extension measuring; S960QL (t20), double-V, G89

The maximum engineering stress is calculated by the following Eq. (5) considering the original cross-sectional area S_0 in the failed region. To consider possible geometrical differences along the parallel length due to remaining weld reinforcement or changes in plate thickness the samples were measured at several points before testing.

$$\sigma_{max} = \frac{F_{max}}{S_0} \tag{5}$$

For the fillet weld tests two extension measurements were performed simultaneously to capture the deformation of both loaded welds, see Figure 4.

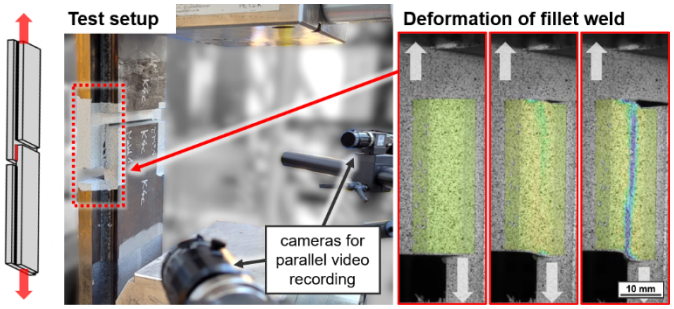

Figure 4 Experimental setup for tensile tests of longitudinal fillet welds with optical local extension measuring

The tested samples were then analysed by 3D measurement (ScanTech, SIMSCAN) of the fracture surfaces to calculate the engineering shear stresses in the longitudinal fillet weld, see Figure 5. The maximum shear stress in the plane of the throat perpendicular to the axis of the weld $\tau_{\parallel,max}$ is derived from the following Eq. (6):

$$\tau_{\parallel,max} = \frac{F_{max}}{A_{frac}} \tag{6}$$

The actual effective throat thickness $a_{3D\text{-}Scan}$ of the penetration fillet welds being based on the measured fracture surface $A_{frac,3D\text{-}Scan}$ and the effective length $l_{eff,w}$ is calculated from Eq. (7).

$$a_{3D\text{-}Scan} = \frac{A_{frac,3D\text{-}Scan}}{l_{eff,w}} \tag{7}$$

The effective throat is analysed to consider the significant difference between the theoretical and actual penetration of the single-run fillet welds.

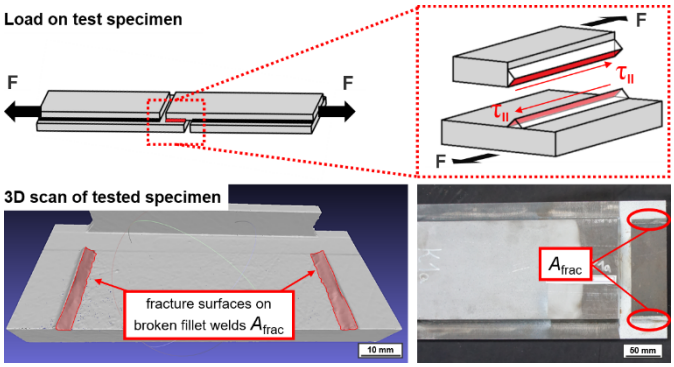

Figure 5 Measurement of fracture surfaces on broken longitudinal fillet welds for determination of shear stresses

3 Results and Discussion

3.1 Macro section and hardness distribution

The fillet welds all show a mitre appearance and good penetration. The measured thickness of the theoretical throat was found to be in the range of 4.7 to 4.9 mm. The formation of a soft zone at the outer HAZ region of the S960QL is evident form the detailed hardness mapping, see Figure 6. An initial hardness level of about 350 HV 0.1 (UCI) was found in the unaltered base material. Near the fusion line in the HAZ a relatively strong hardening of up to about 450 to 470 HV 0.1 (UCI) occurred. Then, the softened zone with an even width of about 1 mm is followed showing a reduced hardness level of about 300 to 340 HV 0.1 (UCI). The weld metal regions show relatively homogeneous hardness distributions and a level depending on the used filler metal. Only little hardness differences in the columnar grain structure are evident resulting from the weld metal solidification and transformation metallurgy. The resulting mean hardness of the weld metal is about 300 HV 0.1 (UCI) for G46, 340 HV 0.1 (UCI) for G69, 435 HV 0.1 (UCI) for G89, and 415 HV 0.1 (UCI) for T89, reflecting their tensile strength.

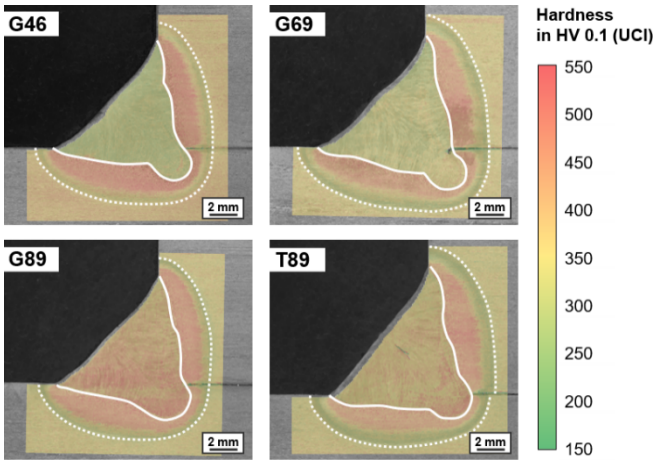

Figure 6 Macro sections of fillet welds on overlap joint of S960QL, Nital etch, with overlaid hardness mapping

In contrast to the single-run fillet welds, a more diverse hardness distribution resulted in the joining area of the butt welds. The resulting HAZ geometry and in particular

the softened zone were formed differently based on the bevel type, see Figure 7.

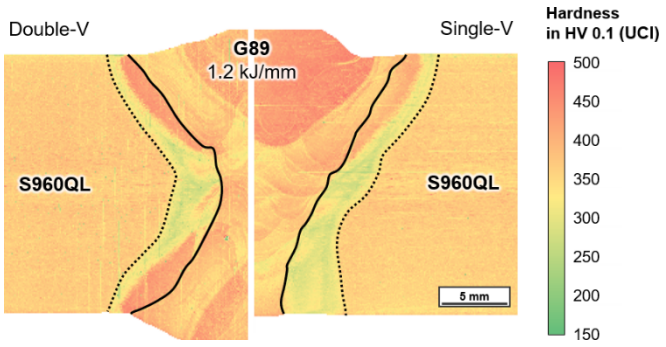

Figure 7 Hardness distribution comparison of butt welded joints of S960QL (t20) using G89 depending on groove type

The multi-pass welding caused a complex formation of HAZ microstructure due to interactive effects of the passed various weld thermal cycles. From the unaltered HAZ of the cover pass a typical hardened area next to the fusion line is apparent representing the grain coarsened (GCHAZ) and fine-grained (FGHAZ) region with quenched micro-structure. Then, a region with reduced hardness level follows representing the intercritical HAZ and subcritical HAZ with tempered microstructure, cf. [4]. In general, a tempering effect inducing a local softening of the subjacent weld bead and its HAZ is evident from the captured hardness distribution. Especially the subcritically reheated FGHAZ of the S960QL is prone to a significant loss of strength deduced by a hardness reduction of up to about –25 %, confirming findings made in other studies on UHSS softening of S960 grades, [7][15]. The closer the layer structure is, the greater is the formed soft zone. This is clearly evident from the root side of the single-V groove in the comparably presented hardness mapping of weld joints of S960QL in Figure 7. The G89 weld metal shows hardness values in the wider range of about 320 to 410 HV 0.1 (UCI) depending on the position in the multi-layered structure. Therefore, the used G89 approved its fitness as matching filler metal even though the nominal tensile strength was lower than that of the base material. The use of the undermatching G46 consumable resulted in a weld metal constitution with clearly lower hardness, see Figure 8.

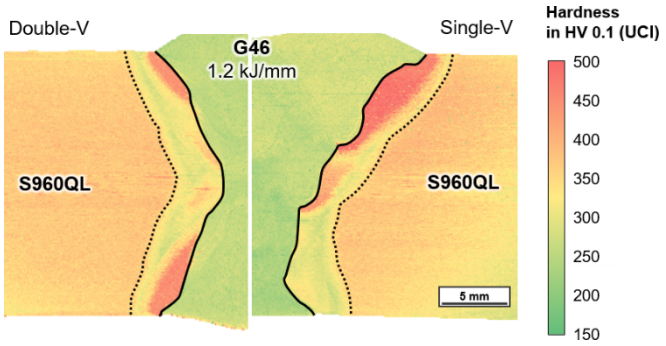

Figure 8 Hardness distribution comparison of butt welded joints of S960QL (t20) using G46 depending on groove type

The resulting hardness level is in the range of about 230 to 280 HV 0.1 (UCI). A higher hardenability results in consequence of the dilution with the higher-alloyed S960QL base material. Despite the assumption that the smaller weld volume of the double-V butts caused a higher degree of dilution related with higher hardenability, an equal hardness level of about 250 HV 0.1 (UCI) in average was found in the weld metal for both groove types. According to this, an increased tensile strength of about 800 N/mm² may be expected, roughly estimated by the conversion tables given in ISO 18265.

Moreover, the diverse material behaviour and weldability of the used UHSSs are apparent from the hardness mapping of butt welded joints with same groove type, weld seam build-up and heat input, but different S960 grades, see Figure 9. Whereas, S960QL forms a typical hardened area in the GCHAZ with hardness values up to about 480 HV 0.1 (UCI), the hardness mapping of S960MC only shows moderate hardening up to about 400 HV 0.1 (UCI). This can be explained by their differing carbon equivalents, cf. Table 2. In addition, the softening susceptibility of S960MC is less pronounced and the HAZ width appears smaller. The differing resistance to softening is due to tempering and transformation effects that depend on the alloy design of the different steel grades, cf. [7][8].

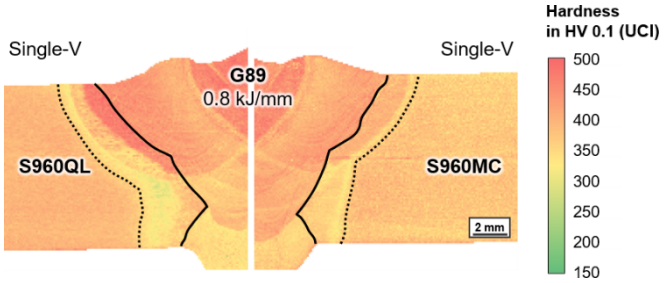

Figure 9 Hardness distribution comparison of single-V butt welded joints of S960QL and S960MC (t10)

From the findings obtained by hardness investigations a different behaviour under tensile load must be expected for the butt welded joints depending on the filler metal as well as the base material grade and groove type. Due to the heterogeneous hardness distribution with softened areas the overall joint behaviour is difficult to predict, and thus must be examined by tensile testing.

3.2 Load-carrying capacity of fillet welds

In contrast to the theoretical throat thicknesses, cf. 3.1, the effective throat thicknesses determined by 3D surface measurement are found to be much larger in the rough range of about 7 to 8.5 mm, see Figure 10 left.

The fillet welds realised with tubular metal cored electrodes T89 tend to have slightly higher effective throat thicknesses, although the arc energy was of the same level as that of welds made with solid wire electrodes ones. This can be caused by a deeper weld bead penetration by GMAW using metal cored electrodes due to the higher current density and deviating material transfer, cf. [19].

Under tensile loading all longitudinal fillet weld samples failed in the weld metal. Both welds showed local deformation in the centre of the weld before the fracture occurred more or less simultaneously under the typical angle of 45°, see exemplarily in Figure 4.

To check the applicability of the current design model regarding the investigated joints characteristic resistance values were compared with loads actually endured. The determined characteristic resistances of the fillet welds

(red dashes in Figure 10 right), based on the design model represented in Eq. (4), were calculated by inserting the actual material properties R_m from Table 1 instead of using the nominal ultimate tensile strengths f_u or $f_{u,FM}$ and, further, neglecting the partial factor.

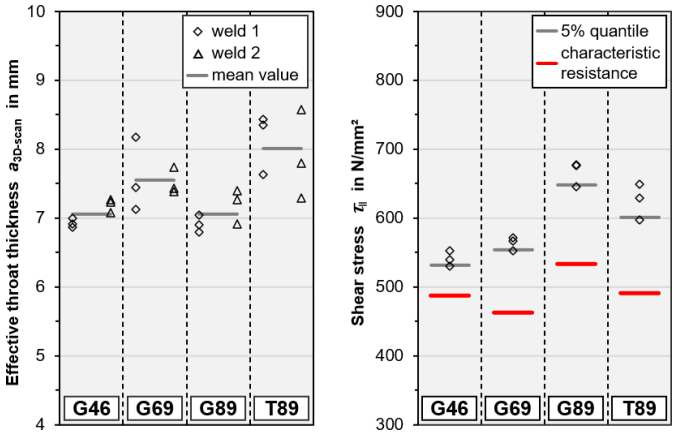

Figure 10 Effective throat thicknesses based on measured fracture surfaces (left) and load-carrying capacity of longitudinal fillet welded S960QL using different filler material (right)

The determined maximum longitudinal shear stresses calculated based on the maximum force and the fracture surface show different levels depending on the filler metal strengths, see data points and derived 5 % quantiles in Figure 10 right. The G89 welds show even higher maximum stresses than the T89 ones which can be explained by its about +12 % higher actual tensile strength, see Table 1. The higher tensile properties of the filler material resulted in higher load-carrying capacities. Nonetheless, due to the resulting stress state only smaller increases are present. The higher strength welds made with G89 and T89 give a little more scatter which might be due to the sporadic occurrence of intercolumnar micro-cracks in the centreline expected to be a solidification cracking phenomenon, see exemplarily T89 fillet weld in Figure 6. Solidification cracking is known to be a relevant issue in welding UHSS in presence of critical combination of mechanical and metallurgical factors, cf. [20][21].
All characteristic resistance values are considerably lower than the 5 % quantiles of the resulting stress values from the tensile tests. This means, the current design model for fillet welds in connections with different parent metal and filler metal strength is suitable to ensure structural integrity for all executed material combinations. However, from the technical point the beneficial use of higher strength consumables, i.e. G69, T89, and G89, is not represented in the design assessment to its full extent. Consequently, the potential higher performance is not adequately considered, and the model seems to be too conservative, at least for the examined single-run welds.

3.3 Load-carrying capacity of butt welds

The obtained maximum engineering stresses from the transverse tensile tests are presented in Figure 11. Additionally, the related 5 % quantiles and the parent metal's ultimate tensile strengths are shown. The associated resistance design values calculated from Eq. (1), but inserting no partial factor and using the actual material tensile strength R_m (Table 1) instead of the nominal strengths f_u and $f_{u,FM}$, are presented by red dashes to verify the design concept. The tensile strength of the quenched S960QL is about +8 % higher than that of the thermomechanically rolled S960MC so that the characteristic resistance value is increased, too.
The undermatching butt welded joints using G46 showed a ductile failure in the weld metal region, after deformation and necking, see Figure 12 a) and c). The determined load-carrying capacity is in the range of about 750 to 850 N/mm², and thus being much lower than the base metal's tensile strength but substantially exceeding the all weld metal strength, see Table 1. This can be explained by the dilution and confirms the expectations based on the hardness investigations. However, the double-V type joints bore slightly higher maximum stresses than the single-V ones. This may be caused by the smaller weld volume in combination with the smaller softened region in the HAZ causing an overall higher strength in the entire joint region. Despite of the lower weld metal strength the undermatched connections can be considered in practice for specific applications to ensure high ductility and toughness or to reduce residual stresses in the welded region.

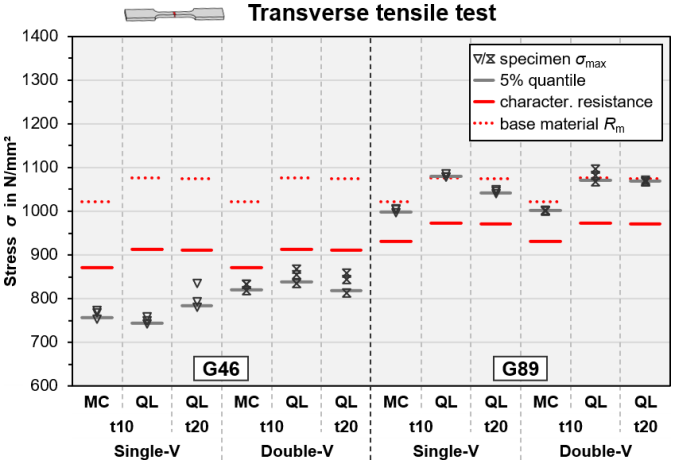

Figure 11 Load-carrying capacity of butt welded joints of S960QL ("QL") and S960MC ("MC") with different thicknesses, groove types and filler material

However, the determined characteristic resistances of the G46 butt welded S960 grades are considerably higher than the investigated maximum engineering stresses. The double-V joints fall below the characteristic resistance values by down to −10 % for S960QL (t20), whereas the single-V butt welds show even higher deviation of −19 % for S960QL (t10). Since these characteristic values are not on the safe side, the design model requires an adjustment for the extension for steel grades up to S960 and under-matching material combination.

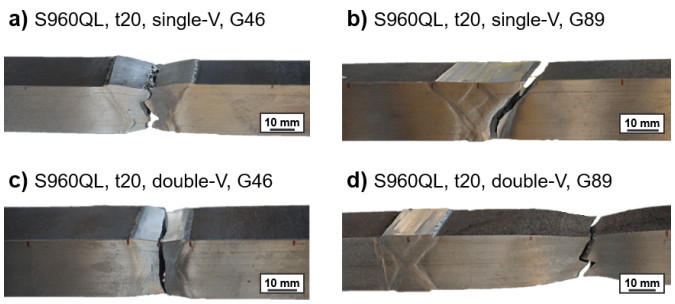

Figure 12 Failure behaviour of butt welded joints of S960QL (t20) depending of groove type and filler material grade

The butt joints welded with the G89 filler bore maximum engineering stresses of about 1000 to 1100 N/mm². The fracture of the S960QL and S960MC specimens occurred for double-V butt welds in the unaltered base material under high elongation and necking, see exemplarily Figure 12 d). This means that the used G89 solid wire electrode can be considered as matching filler material as expected from the actual mechanical properties of the used consumable, see Table 1. Initially, the deformation mainly occurred locally in the softened region of the HAZ, but for further tension development the major elongation and subsequent failure were present in the unaltered base metal, see exemplarily local deformation image sequences in Figure 3 right. The S960QL single-V butt joints with t = 10 mm and 20 mm, welded with G89, failed diagonally through the HAZ region with only little necking, see exemplarily Figure 12 b). This is caused by the distinctive soft zone formation due to the one-sided multi-pass welding procedure, as identified from the hardness investigations, see Figure 7 right. Only the thicker S960QL (t20) single-V joint samples failed all at a slightly reduced maximum engineering stress compared to the parent metal ultimate tensile strength.
The derived 5 % quantiles of the maximum engineering stresses are all above the determined characteristic resistance values in the even range of +8 to +11 % so that the design model was found to be on the safe side. The use of the quasi-matching filler metal G89 is already well represented for steel grade S960 in the current design concept according to Eq. (1).

4 Conclusions and outlook

Since the current design concepts of Eurocode 3 do not represent the use of UHSSs of S960 grades, investigations were made on the weldability and resulting load-bearing capacities of GMAW transverse butt welds and longitudinal fillet welds. Hardness distribution analysis in the cross section of the joints and tensile tests were performed. The following conclusions were drawn from the results:

a) A softening effect occurs in the HAZ of the UHSS. The form and characteristics of the soft zone depend on the steel grade, i.e. alloy design, delivery condition, as well as the weld joint configuration. The subcritically reheated regions of subjacent bead's HAZ in the S960QL show significant loss of hardness up to –25 %. The thermomechanically rolled S960MC have a better metallurgical weldability and has shown to be less prone to softening.
b) For the investigated butt joints of t = 10 mm and 20 mm the double-V groove facilitates better weldability due to the smaller soft zone formation. Whereas, the one-sided multi-pass welding of the single-V groove causes an increased softening in the HAZ on the root side, so that the failure occurred in the HAZ even when using a matching filler metal.
c) For butt welded joints of S960QL and S960MC using the quasi-matching filler material G89, the design model that is considered in the FprEN 1993-1-8:2023 is on the safe side. When using the undermatching filler material G46, the design model requires an adjustment for the extension up to S960.
d) The load-carrying capacity of longitudinal fillet welds made with different parent metal and filler material strength are covered by the corresponding design model of the FprEN 1993-1-8:2023, but it does not represent the increased performance of higher strength filler materials to its full extent.

For a safe application of S960 weld joints performed with a significant undermatching filler material, the extension of the current design model up to S960 for butt welds needs an adaption. Whereas, an extension of the current design model for fillet welds up to S960 grades is possible because it was found to be on the safe side. However, the higher performance of the fillet welds on UHSS is not adequately considered. To justify adoptions of the current model with regard to higher material utilization more experimental results and statistical analysis are required. Since the multi-pass welding causes a complex HAZ and weld metal metallurgy exercising an influence on the hardness distribution, further investigations on the influence of multiple weld passes should be made for fillet welds, too.
Moreover, to allow the design of UHSS joints with matching filler metal in general the classification of standardized consumables should be extended to strength classes above "89".

5 Acknowledgement

The IGF project "Effective design concepts for welded mixed connections in steel structures" (21412 BG/P 1507) of the Research Association for Steel Application e. V. (FOSTA), Sohnstraße 65, 40237 Düsseldorf, Germany, is a sub-project of the FOSTA joint research program HOCHFEST and was funded by the Federal Ministry for Economic Affairs and Climate Action via the AiF within the framework of the programme for the promotion of joint industrial research and development (IGF) on the basis of a resolution of the German Bundestag. Special thanks go to the industrial partners of the project committee for their support of the research project.

References

[1] Cai, W.-Y.; Wang, Y.-B.; Li, G.-Q.; Stroetmann, R. (2022) *Comparative study on strength of TMCP and QT high strength steel butt-welded joints*. J Constr Steel Res 197, 107447. DOI: 10.1016/j.jcsr.2022.107447

[2] Mičian, M.; Frátrik, M.; Kajánek, D. (2021) *Influence of Welding Parameters and Filler Material on the Mechanical Properties of HSLA Steel S960MC Welded Joints*. metals 11, 305. DOI: 10.3390/met11020305

[3] Keränen, L.; Nousiainen, O.; Javaheri, V.; Kaijalainen, A. et al. (2022) Mechanical *properties of welded ultrahigh-strength S960 steel at low and elevated temperatures*. J Constr Steel Res 198, 107517. DOI: 10.1016/j.jcsr.2022.107517

[4] Afkhami, S.; Javaheri, V.; Amraei, M.; Skriko, T.; Piili, H.; Zhao, X.-L.; Björk, T. (2022) *Thermo-mechanical simulation of the heat-affected zones in welded ultra-high strength steels: Microstructure and mechanical properties*. Mater Des 213, 110336. DOI: 10.1016/j.matdes.2021.110336

[5] Björk, T.; Toivonen J. (2012) *Capacity of Fillet Welded Joints Made of Ultra High-Strength Steel*. Weld World 56, 71-84. DOI: 10.1007/BF03321337

[6] Spiegler, J. (2022) *Tragfähigkeit von Kehlnaht- und Stumpfnahtverbindungen höherfester Baustähle*. Dissertation. Mitteilung Institut für Konstruktion und Entwurf No. 2022-2, University of Stuttgart. DOI: 10.18419/opus-12207

[7] Zhang, L.; Kannengiesser, T. (2016) *HAZ softening in Nb-, Ti- and Ti + V-bearing quenched and tempered steel welds*. Weld World 60, 177–184. DOI: 10.1007/s40194-016-0299-7

[8] Schaupp, T.; Schroepfer, D.; Kromm, A.; Kannengiesser, T. (2017) *Welding* residual *stresses in 960 MPa grade QT and TMCP high-strength steels*. J Manuf Process 27, 226–232. DOI: 10.1016/j.jmapro.2017.05.006

[9] DIN EN 1993-1-1:2010-12 (2010) Eurocode *3: Design of steel structures - Part 1-1: General rules and rules for buildings*; German version EN 1993-1-1:2005 + AC:2009

[10] DIN EN 1993-1-8:2010-12 (2010) *Eurocode 3: Design of steel structures - Part 1-8: Design of joints*; German version EN 1993-1-8:2005 + AC:2009

[11] DIN EN 1993-1-12:2010-12 (2010) *Eurocode 3: Design of steel structures - Part 1-12: Additional rules for the extension of EN 1993 up to steel grades S700*; German version EN 1993-1-12:2007 + AC:2009

[12] FprEN 1993-1-8:2023 (2023) *Eurocode 3 – Design of steel structures – Part 1-8: Joints*. Formal Vote Version. European Committee for Standardization

[13] CEN/TC 250/SC 3/WG12 N118 (2021) *prEN 1993-1-12: Eurocode 3 – Design of steel structures – Part 1-12: Additional rules for steel grades up to S960*. Working Draft (unpublished). European Committee for Standardization

[14] DIN EN 1011-2:2001-05 (2001) *Welding - Recommendation for welding of metallic materials - Part 2: Arc welding of ferritic steels*; German version EN 1011-2:2001

[15] Amraei, M.; Ahola, A.; Afkhami, S.; Björk, T.; Heidarpour, A.; Zhao, X.-L. (2019) *Effects of heat input on the mechanical properties of butt-welded high and ultra-high strength steels*. Eng Struct 198, 109460. DOI: 10.1016/j.engstruct.2019.109460

[16] DVS-Merkblatt 0916 (2012) *Metall-Schutzgas-schweißen von Feinkornbaustählen*. Technical bulletin. Düsseldorf: DVS Media GmbH

[17] von Arnim, M.; Eichler, S.; Brätz, O.; Hildebrand, J.; Gericke, A.; Kuhlmann, U.; Bergmann, J.P.; Flügge, W. (2022) *Effiziente Nachweiskonzepte für geschweißte Mischverbindungen im Stahlbau*. Stahlbau 91, 10, 660-670. DOI: 10.1002/stab.202200046

[18] Schneider, C.; Ernst, W.; Schnitzer, R.; Staufer, H.; Vallant, R.; Enzinger, N. (2018) *Welding of S960MC with undermatching filler material*. Weld World 62, 801–809. DOI: 10.1007/s40194-018-0570-1

[19] Starling, C.M.D.; Modenesi, P.J.; Borba, T.M.D. (2010) *Comparison of operational performance and bead characteristics when welding with different tubular wires.* Weld Int 24, 8, 579-592, DOI: 10.1080/09507110903568810

[20] Saadati, M.; Nobarzad, A.K.E.; Jahazi, M. (2019) *On the hot cracking of HSLA steel welds: Role of epitaxial growth and HAZ grain size*. J Manuf Process 41, 242-251. DOI: 10.1016/j.jmapro.2019.03.032

[21] Chen, Z.; Xiong, Y.; Qiu, H.; Lin, G.; Li, Z. (2018) *Stress intensity factor-based prediction of solidification crack growth during welding of high strength steel.* J Mater Process Technol 252, 270-278. DOI: 10.1016/j.jmatprotec.2017.09.031